2021 43rd Annual International Conference of the
IEEE Engineering in Medicine & Biology Society (EMBC)
Oct 31 - Nov 4, 2021. Virtual Conference

Optical Fiber Coupling System for Steerable Endoscopic Instruments

Mingzhang Zhu, Yao Shen, Alex J. Chiluisa, Jialin Song, Loris Fichera, and Yuxiang Liu

***Abstract*— In this paper, we present an optical coupling system that couples light from an Endostat fiber in a commercial laser surgical system into a smaller multimode fiber, in order to enable endoscopic probe steering in a tightly confined space. Unlike the Endostat fibers, which have a minimum bending radius of 12 mm due to the large diameter, our work allows the laser to be delivered by smaller fibers that can be readily bent at a 6-mm bending radius by a distal steerable mechanism. Such a readily achievable sharp bending facilitates the surgical laser to access hard-to-reach anatomies. We experimentally achieved an optical power coupling efficiency of ≈ 50%. Tissue ablation experiments were performed to prove the feasibility and potential of our light coupling system in clinical laser surgeries, as well as other optical fiber-based endoscopic medical devices.**

***Clinical Relevance*— Optical fibers are commonly used in laser-based surgical systems. The optical coupling system in this paper enables the laser to be delivered by small fibers, helps realize the fiber bending and steering, and hence allows the laser treatments of previous inaccessible anatomies.**

I. Introduction

With the benefits of precise tissue removal and effective hemostasis, the laser has been widely implemented to replace scalpels in general surgeries including endarterectomy, lipectomy, and gingivectomy. Additionally, the integration of optical fibers with flexible endoscopes provides an exciting method to perform treatments of internal anatomies that are difficult to access, such as laser ablation of laryngeal lesions [1], as shown in Fig. 1 (a). This procedure can significantly reduce the cost and rehabilitation period with minimal incisions while enhancing safety [2-4]. However, a non-steerable fiber inside a flexible endoscope, which is commonly used, can only treat lesions located on the straight path and aimed against the endoscope [5]. The limited accessible area of the fiber-delivered laser hinders the applications of this procedure.

The steering distal mechanism is a potential solution to tackle the above challenge. Recent work on the simulation of a steerable-probe laser demonstrated the capability to access more than 70% larynx area than along-the-axis laser in a non-steerable fiber probe, as shown in Fig.1 (c) [6]. This simulation indicates that the steerable laser surgical probes can treat some of the patients who cannot be treated otherwise. However, several technical challenges blocked the clinical implementation of this steerable probe. One major challenge is the absence of suitable fibers, which require minimized

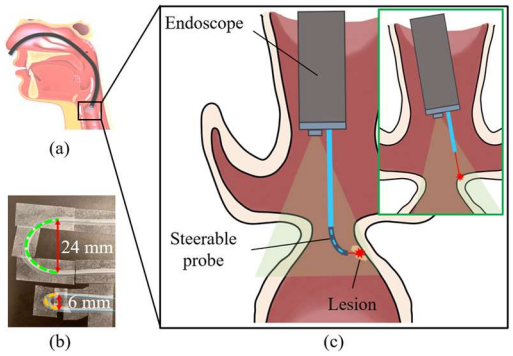

Figure 1. (a) Schematic of the flexible endoscopic device inserted into the larynx through the nose. (b) Comparison of the minimum bending diameter between an Endostat fiber (Green dashed line) and a 200 μm multimode fiber (Yellow dashed line). (c) Schematic of a steerable probe that is able to treat lesions facing downward and inside laryngeal ventricles. (Inset) Schematic of a non-steerable endoscope with the forward-looking probe that can only reach tissue areas facing up.

diameter and bending radius to reach sophisticated and narrow anatomies [7]. However, most of surgical lasers (PDL, CO2, KTP) have a relatively thick fiber core (> 0.4 mm in diameter) [8], and thus suffer from a large bending radius (> 3 cm), as shown in Fig.1 (b), which results in a limited steering angle of distal mechanism. To overcome the above challenge, a practical solution that enable the usage of laser-induced steering mechanism is required eagerly.

In this paper, we developed an optical fiber coupling system that couples a high-power laser from a commercial surgical fiber to a flexible, thinner multimode fiber for laser surgeries. This system provides a convenient approach to emit a green laser (532 nm) from a thin enough fiber to allow a sharp bending radius of 6 mm. In addition, the thinner fiber is easier to be bent by a steering probe mechanism. The above benefits pave the way for potential steerable fiber-based laser probes in clinical applications. We experimentally measured the coupling efficiency to be ≈ 50%. To further evaluate the performance of our system in laser surgeries, we conducted an experimental parametric study of the laser removal of a tissue-mimicking agar at different optical powers. The results prove that the laser emitted from the 200 μm multimode fiber through our coupling system was powerful enough to remove the agar, which indicates the feasibility of our coupling system in clinical applications. This research sheds light on addressing the challenges of bending commercial thick fibers with diameters > 0.4 mm in endoscopic instruments, such as arthroscopic procedures [9].

Research reported in this paper was supported by the National Institute on Deafness and Other Communication Disorders of the National Institutes of Health under award number R15DC018667. The content is solely the responsibility of the authors and does not necessarily represent the official views of the National Institutes of Health.

All authors are with Worcester Polytechnic Institute, MA 01609 USA
Corresponding author: Mingzhang Zhu (phone: 508-335-8054; e-mail: mzhu@wpi.edu).

II. Design and Method

As shown in Fig. 2 (a), the laser coupling system consists of two main components, a reflective collimator (RC08FC-P01, Thorlabs) and an achromatic straight collimator (F950FC-A, Thorlabs). The laser emitted from Aura-i Laser System (Boston Scientific, Marlborough, MA) is transmitted through an Endostat Fiber (10-0632, American Medical Systems) with a core diameter of 0.4 mm. The Endostat fiber is able to deliver laser energy at both 532 nm and 1064 nm. The reflective collimator was used to collimate the laser emitted from the Endostat fiber. The parallel rays coming from the reflective collimator was coupled into the step-index multimode fiber (FP200ERT, Thorlabs) through the second straight collimator. This thinner multimode fiber (0.5 NA, 200 µm core, 225 µm cladding) is only a half diameter of the Endostat fiber, which allows a sharper bending radius and requires a smaller force moment to bend for the purpose of the steerable laser probe. The 0.5 NA allows the multimode fiber to collect the focused light from the straight collimator. We chose to use collimators over a lens-based cage system because the size of our system is more compact, and the separation between two collimators can be easily adjusted, both of which enhance the system's flexibility and robustness and are preferred in clinical uses.

To select the components in the design, we first measured the numerical aperture (NA) of the Endostat fiber experimentally. The red laser (1064 nm) was used for its relatively low output power compared with the green laser (532 nm) to avoid saturated optical measurements. The NA difference between the two wavelengths in the same fiber was experimentally measured to be < 10%. As shown in Fig. 3, an observation screen (EDU-VS2, Thorlabs) was placed in front of the fiber end in a predefined axial distance, L. The divergent beam profile generated on the screen is captured by a camera, as shown in Fig. 4 (a). The intensity profile was fitted by a Gaussian distribution, as shown in Fig. 4 (b). We define the spot size, D, as the Full Width Half Maximum (FWHM). We defined partial spot size, x, as (D – d)/2, where d is the fiber core diameter. θ is the half divergence angle. The NA of the fiber is defined as in (1):

$$NA = \sin\theta = sin\,(\tan^{-1}(x/L)) \quad (1)$$

We repeated the measurements at different axial distances (5 mm – 20 mm) to obtain the dependence of the spot size on the axial distance, as shown in Fig. 4 (c). From the linear fit, we were able to estimate the NA of the Endostat Fiber to be 0.383, which determined a critical parameter for selecting the reflective collimator.

To acquire the optimal coupling efficiency, both the multimode fiber and Endostat fiber need to be well terminated with mirror-like end faces, which was achieved by the polishing method. First, the fiber end was stripped, cleaved, and mounted with an FC/PC connector. The fiber tip was then polished by successive polishing discs with decreasing roughness (12 µm grit, 3 µm grit, and 1µm grit in sequence). The typical polished fiber end tips are shown in Fig. 2 (b).

The straight collimator was mounted on a standard cage plate (CP02, Thorlabs), and the reflective collimator was fixed on a three-dimensional (3D) manual stage with a kinematic mount, which provides translational and angular adjustment.

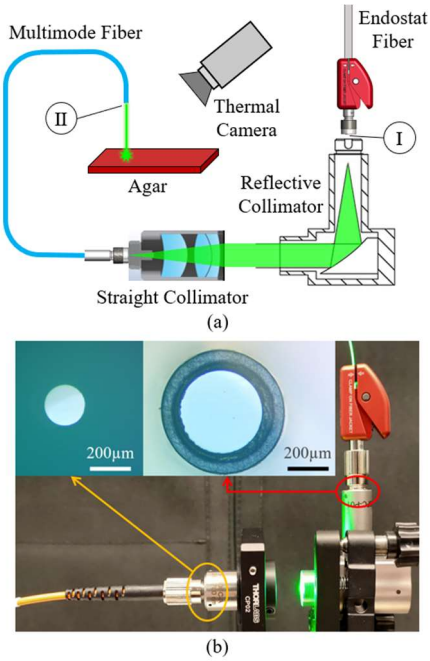

Figure 2. (a) Schematic of the laser coupling system. The Roman numerals balloons are I: Location of input power measurement; II: Location of output power measurement. (b) Experimental setup of the laser coupling system where KTP laser was coupled from the Endostat fiber into the multimode fiber. (Left inset) Microscope image of the 200 µm multimode fiber polished end face. (Right inset) Microscope image of the Endostat fiber polished end face.

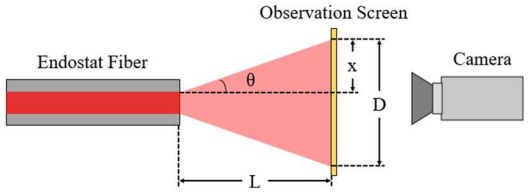

Figure 3. Schematic of the NA measurements of the Endostat fiber.

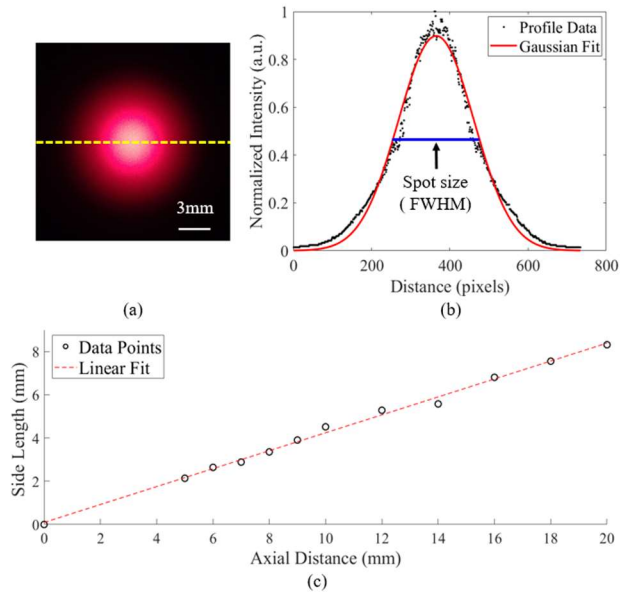

Figure 4. (a) Camera image of a light spot on the screen at an axial distance = 6 mm. (b) The intensity profile (black dots) along the yellow dashed line in (a). The red curve represents the Gaussian fit. The blue line represents the spot size (FWHM). (c) Dependence of the partial spot size (side length) on the axial distance. The red dashed line represents the linear fit of the data.

The position of the reflective collimator was adjusted to ensure that the axis of input port of the straight collimator is coaxial with that of the output port of reflective collimator. The optical transmission was monitored in the real time of the alignment to ensure an optimal transmission efficiency.

III. Results

A. Coupling Efficiency at Different Optical Powers

To evaluate the performance of our coupling system, we measured the power of the green laser at different locations in the coupling system and calculated the coupling efficiencies (CEs), as shown in Table. 1. The bare fiber or FC/PC connector of interest was inserted into an optical power meter (S302C, Thorlabs and PM100D, Thorlabs) for power measurements. We measured the laser emitted from the Endostat fiber as the input power, and the laser emitted from the multimode fiber as the output power. The exact locations of measurements are shown in the Roman numeral balloons in Fig. 2 (a). The CE is defined as in (2):

$$\text{CE} = (\text{Output Power}) / (\text{Input Power}) \times 100\% \qquad (2)$$

The set power is the nominal power shown on the front panel of the Aura-i Laser System, and we will use the set power in the rest of the paper to refer to the nominal output power. The range of the set power was 0.5 W to 4 W, which was limited by the maximum measurable power of the power meter. The measurements reported in Table I have a shared uncertainty of +-0.001 W, and the sources of this uncertainty include the laser source power fluctuations and the power meter resolution.

TABLE I. POWER MEASUREMENTS AT DIFFERENT LOCATIONS

Set Power (W)	Input Power (W)	Output Power (W)	Coupling Efficiency (%)
0.5	0.365	0.190	52.05
0.6	0.440	0.225	51.14
0.7	0.525	0.255	48.57
0.8	0.595	0.315	52.94
0.9	0.675	0.365	54.07
1	0.760	0.410	53.95
2	1.495	0.815	54.52
3	2.290	1.085	47.38
4	3.090	1.495	48.38

The results show that, at different setup powers, our coupling system had an average CE of 51.44% with a standard deviation of 2.60%. The measured CE proved that our coupling system was capable to deliver laser energy with a reasonable loss. The independence of CE on the laser power is beneficial to the surgery because the laser power delivered to the tissue can be well predicted when doctors need to adjust the power at the laser source.

B. Laser-induced Damage on Tissue-Mimicking Agar

By using our coupling system with the commercial Aura-i laser source, we evaluated the laser-induced damages on a homemade tissue-mimicking agar. The agar was made by mixing 2 g agar powder (Sigma-Aldrich, A1296, USA), which has been verified to mimic soft tissue [10], 100 g distilled water, and 2 g red dye. We placed the 200 µm multimode fiber tip about 1.5mm above the surface of agar and input a single laser pulse with a duration of 0.5 second in a power range of 0.5 W – 5 W, which formed circular shallow pits in the agar.

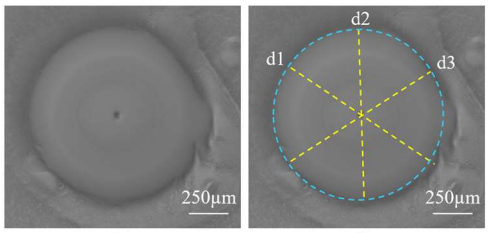

Figure 5. (a) Microscope image of the laser-removed pit in the agar at a 3.5 W set power. (b) Pit diameter measurements. The blue dash circle represents the estimated pit boundary. The yellow dash lines represent three independent diameter measurements.

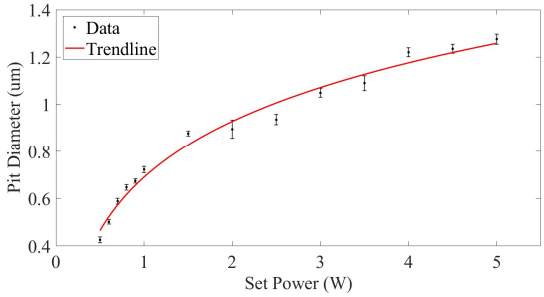

Figure 6. Dependence of the pit diameter on set power.

Two parameters were investigated to characterize the laser-induced damages on agar: pit diameter and temperature of the target area, as detailed below.

1) Pit Diameter Measurements

We used a digital microscope (VHX-7000, KEYENCE) to image the pit area, as shown in Fig. 5 (a). The shaded boundary of the pit was considered to be the pit diameter, as shown in Fig. 5 (b). Because of the imperfect circular shape, three diameters along different orientations were measured on the same pit to obtain statistical results, as shown in Fig. 5 (b). The diameter measurements have an uncertainty of +-0.01 mm, and the source of this uncertainty is the manual selection of the diameter ends.

The relationship between the pit diameter and the set power is depicted in Fig. 6. The pit diameter increases from 0.4 mm to 1.3 mm when the set power is increased from 0.5 W to 5 W. No threshold value, i.e., minimal power to cause damage, was observed in this experiment. According to these results, the green laser emitted from the 200-µm fiber through the laser coupling system was able to cause photo damages and remove the agar with a power range of 0.5 W – 5 W.

2) Laser-induced Agar Temperature Measurements

In addition to the size of the laser-removed agar, we used a thermal camera (A655sc, FLIR) to measure the temperature in the laser illuminated area on the agar, in order to characterize quantitively the laser effects. Since the boiling point of the agar is approximately 90 °C, temperature measurement reaching this boiling point is categorized to be burned. A heat map of the agar imaged by the thermal camera is shown in Fig. 7. Fig. 8 (a) shows the time series of maximum temperature of the target area over the 0.5-second duration of the laser pulse. The plot presents that the temperature in the Region of Interest (ROI) kept increasing during the laser illumination, followed by a sharp drop when the laser was turned off.

By repeating the measurements at different set powers, we

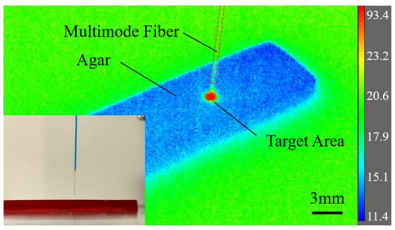

Figure 7. Temperature map of the agar in 2 W set power. (Inset at lower left corner) Regular camera image showing the relative position of the multimode fiber on the agar.

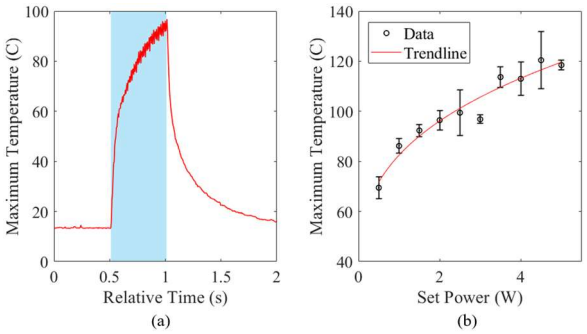

Figure 8. (a) Time series of the maximum temperature of the ROI at a 2 W set power. The blue shaded area represents the period (0.51 – 1.01 seconds) when the laser was on. (b) Dependence of the maximum temperature on set power.

found that the maximum temperature increased with the set power, as shown in Fig. 8 (b). The threshold set power to burn the agar was found to be 2.5 W. For the data points over 90 °C (3.5 W – 5 W), we speculated that these temperatures occurred at the solid debris left inside the pit without water.

The results show that the laser through our coupling system was able to ablate the agar, which proves that the CE of our coupling system is sufficient for surgical applications.

C. Characterization of the Bending-induced Power Loss with the 200-µm Multimode fiber

To evaluate the advantages of delivering light in the smaller fiber through our coupling system, we inserted the 200 µm multimode fiber into a miniaturized steerable probe, as shown in Fig. 9. The steerable probe had a bending radius, R, of ~ 6 mm at a 90-degree bending angle. Such a bending radius cannot be achieved with the commercial Endostat fiber due to the large fiber size. In our experiment, the minimum bending radius of the Endostat fiber was 12 mm before it was broken. By comparing the optical powers emitted from the fiber tip before and after the fiber was bent, we found only 4.5% power loss was induced by bending the fiber at a 6-mm bending radius. These results clearly demonstrate the advantages of our coupling system and the fiber steering in a tight space, such as a larynx.

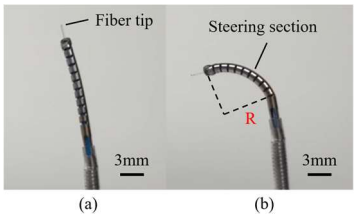

Figure 9. Steerable probe with 200-µm multimode fiber (a) at a straight position and (b) at a 90-degree bending position with a bending radius of R = 6 mm.

IV. Discussion

As shown above, there were over 40% of power lost in the laser coupling system. The possible reasons include the following. (1) The Endostat fiber NA (0.383) is larger than our current reflective collimator NA (0.167), so part of the light was not collimated properly. (2) Dust flying in the air could adhere to the 200 µm multimode fiber end face, which caused the scattering of light. (3) There existed an alignment error between the collimators. Potential improvements include a different reflective collimator with a better matching NA, improvements in the alignments, and careful cleaning and checking of the fiber end faces.

One major limitation that hinders the application of our coupling system in clinical laser surgeries is that end faces on both sides of the 200 µm multimode fiber were easily damaged by the high optical power. In our experiments, at a 1 W set power, the coupling efficiency started to decline after 15-20 seconds of continuous laser illumination due to the end face photo damage. The impaired end face needed to be cleaned and repolished to restore the optical transmission efficiency. One potential solution is to connect the thick and thin fibers by fiber tapering and splicing techniques, which avoid the fiber-to-free-space light coupling in the coupling system. Research in this direction is underway.

We are working on integrating the optical coupling system with the steerable probe mechanism. We plan to bring the integrated system to clinical offices to test the real-world performance in laser surgeries.

References

[1] L. Fichera, “Bringing the light inside the body to perform better surgery,” Science Robotics, vol. 6, no. 50, 2021.

[2] C. Y. Kuo and S. L. Halum, “Office-Based Laser Surgery of the Larynx: Cost-Effective Treatment at the Office’s Expense,” Otolaryngology-Head Neck Surg, vol. 146, no. 5, pp. 769–773, 2012.

[3] M. Amin, Office Procedures in Laryngology, An Issue of Otolaryngologic Clinics Elsevier Health Sciences, 2012.

[4] K. O’Brien, Z. R. Boyer, B. G. Mart, C. T. Brolliar, T. L. Carroll, and L. Fichera, “Towards Flexible Steerable Instruments for Office-Based Laryngeal Surgery,” presented at the 2019 Design of Medical Devices Conference, doi: 10.1115/DMD2019-3309, 2019.

[5] A. Del Signore, R. Shah, N. Gupta, K. Altman, and P. Woo, “Complications and Failures of Office-Based Endoscopic Angiolytic Laser Surgery Treatment,” Journal of voice : official journal of the Voice Foundation, vol. 30, no. 6, pp. 744–750, 2015.

[6] I. A. Chan, J. F. d’Almeida, A. J. Chiluisa, T. L. Carroll, Y. Liu, and L. Fichera, “On the merits of using angled fiber tips in office-based laser surgery of the vocal folds,” in Medical Imaging 2021: Image-Guided Procedures, Robotic Interventions, and Modeling, vol. 11598, p. 115981Z, 2021.

[7] M. Runciman, A. Darzi, and G. P. Mylonas, “Soft Robotics in Minimally Invasive Surgery,” Soft Robot, vol. 6, no. 4, pp. 423–443, 2019.

[8] C. Ayala, M. Selig, W. Faquin, and R. A. Franco, “Ultrastructural Evaluation of 585-nm Pulsed-Dye Laser-Treated Glottal Dysplasia,” Journal of Voice, vol. 21, no. 1, pp. 119–126, 2007.

[9] Z. Long, K. Nagamune, R. Kuroda, and M. Kurosaka, “Real-Time 3D Visualization and Navigation Using Fiber-Based Endoscopic System for Arthroscopic Surgery,” Journal of Advanced Computational Intelligence and Intelligent Informatics, vol. 20, no. 5, pp. 735–742, 2016.

[10] A. I. Chen et al., “Multilayered tissue mimicking skin and vessel phantoms with tunable mechanical, optical, and acoustic properties,” Medical Physics, vol. 43, no. 6, pp. 3117–3131, 2016.